The elasticity of single kettin molecules using a two-bead laser-tweezers assay

Mark C. Leake[a,*], David Wilson[b], Belinda Bullard[c], Robert M. Simmons[b]

[a] *The Randall Centre for Molecular Mechanisms of Cell Function, King's College London, New Hunt's House, Guy's Campus, London SE1 1UL, UK*
[b] *MRC Muscle and Cell Motility Unit, King's College London, New Hunt's House, Guy's Campus, London SE1 1UL, UK*
[c] *European Molecular Biology Laboratory, Postfach 10.2209, 69012 Heidelberg, Germany*

Received 5 November 2002; revised 9 December 2002; accepted 13 December 2002

First published online 24 December 2002

Edited by Michael R. Bubb

Abstract Kettin is a high molecular mass protein of insect muscle associated with thin filaments and α-actinin in the Z-disc. It is thought to form a link between thin and thick filaments towards its C-terminus, contributing significantly to passive sarcomere stiffness. Here the elastic properties were characterised by mechanical stretches on an antibody-delimited region of the single molecule using two independent optical traps capable of exerting forces up to 150 pN. Step-like events were observed in the force–extension relationships consistent with the unfolding of Ig domains at moderate force and refolding of these domains at significantly higher forces than have been observed for related modular proteins.

Key words: Laser-tweezers; Kettin; Single molecule manipulation; Unfolding/refolding; Entropic spring

1. Introduction

Kettin is a high molecular mass protein expressed in insect muscle [1,2]. The cDNA sequence of *Drosophila* kettin [3,4] encodes a polypeptide of ~500 kDa with a modular structure, showing similarities to titin-like proteins but possessing no fibronectin type III (Fn3), kinase or PEVK domains. It consists of 35 modules having homology only to immunoglobulin (Ig)-like domains of ~100 residues length, most of which are linked by putatively random coil sequences of ~35 residues except near the N- and C-termini where linkers are either very short or missing entirely.

In flight muscle, the N-terminus of kettin is located in the Z-disc, the molecule running along an actin thin filament with the C-terminus located some way beyond the Z-disc [5]. Kettin binds strongly to actin thin filaments with a stoichiometry of one Ig domain per actin protomer [5,6] and may act as an anchor for the thin filament system at the Z-disc through tight binding of adjacent, oppositely polarised molecules via α-actinin. Recent evidence [7] suggests that a C-terminal region of the molecule of undetermined length is firmly attached to the thick filament, and that part of the kettin molecule is free to extend upon the imposition of external force, thereby contributing to the passive stiffness of the insect sarcomere.

Drosophila kettin is a product of differential splicing from the *D-titin* gene, also called the *sls* gene [8,9,32]. It has similarities to vertebrate titin [10,11] and *Drosophila* projectin [12,13], in which alternative splicing leads to several tissue-specific isoforms. *Drosophila* kettin of indirect flight muscle for example exists in two known isoforms, ~500 kDa and a less common ~700 kDa variety. The isoform variation in the vertebrate titin system is known to result in a different passive stiffness for myofibrils of different muscle types, specific to the physiological demands of that muscle. It is possible therefore that kettin, perhaps in combination with projectin, may act in a similar way. Also, if there is a region of the kettin molecule which is free to extend in the sarcomere, it is possible that the imposition of sustained external force may result in the unfolding of one or more Ig domains, as has been speculated for the case of vertebrate titin [14–18], and if so may suggest a potential role as shock-absorber. In the present study it is confirmed that single kettin molecules denature upon the imposition of force in a manner consistent with the unfolding of the Ig domains, and it is in addition shown that refolding occurs at relatively high forces, which may have significant implications for the physiological system.

2. Materials and methods

2.1. Extraction and purification of kettin and production of anti-kettin antibodies

Kettin (500 kDa) was isolated from *Lethocerus* leg muscle as previously described [5]. Polyclonal antibodies were raised in rabbits to two constructs: KET1 and KET2, derived from the *Drosophila* sequence. KET1 is Ig3 plus half of Ig4 and KET2 is Ig24-linker-Ig25; the Ig numbers are as in [4], KET1 and KET2 are separated by 19 complete Ig-linker modules (Fig. 1A). Specific IgG was isolated from serum on an affinity column of the peptide coupled to CM-Sepharose (Pharmacia); IgG was eluted at pH 4.0 [5].

2.2. Bead and flow-cell preparation

Aldehyde-derivatised latex beads (Interfacial Dynamics Corporation, Oregon, USA) of 2.0 μm diameter were incubated at 1% (w/v) in 10 μg/ml of either KET1 or KET2 antibody solution in phosphate-buffered saline (PBS), pH 7.4, 22°C for 1 h. For KET1 bead preparations 0.1 μM rhodamine isothiocyanate (RITC) was added 5 min prior to the end of incubation. The beads were sonicated for 5 min, washed once, resuspended at 1% (w/v) in 1 mg/ml bovine serum albumin (BSA) and incubated for a further 30 min to block unreacted aldehyde sites. They were then washed and spun again three times,

*Corresponding author. Present address: University of Heidelberg, Institute of Physiology and Pathophysiology, Im Neuenheimer Feld 326, D-69120 Heidelberg, Germany. Fax: (49)-6221-544039.
E-mail address: m.leake1@physics.ox.ac.uk (M.C. Leake).

Abbreviations: AOM, acousto-optic modulator; BSA, bovine serum albumin; FJC, freely jointed chain; Fn3, fibronectin type III; Ig, immunoglobulin; QD, quadrant photodiode; RITC, rhodamine isothiocyanate; WLC, worm-like chain

0014-5793/03/$22.00
doi:10.1016/S0014-5793(02)03857-7

resuspended at 0.5% (w/v) in PBS and stored on ice, the final suspension being designated either KET1-beads or KET2-beads as appropriate.

KET2-beads were spun down and resuspended at 1% (w/v) in a 0.1 μg/ml solution of kettin pre-microdialysed into PBS and incubated overnight on an agitator at 4°C giving a kettin surface density of ~20 molecules/bead. Prior to use these kettin-beads were microdialysed against PBS and stored on ice at 0.5% (w/v). Kettin-beads were then mixed with an equal volume of KET1-beads and diluted by 1:100 in PBS to form the final bead trapping suspension. A flow-cell was prepared consisting of a glass coverslip coated in nitrocellulose (0.1% in amyl acetate, air-dried) stuck to a glass slide via two strips of double-sided tape, giving an inclusive volume of 30–40 μl. One volume of 1 mg/ml BSA was injected into the flow-cell and incubated for 5 min to block the coverslip surface, and was then washed through with three volumes of PBS. One volume of the bead trapping suspension was then injected.

2.3. Laser-tweezers system and calibration

A 2 W near infrared laser (Nd:YLF 1.047 μm TFR, Spectra Physics) was used, the beam split and recombined by polarising beam-splitting cubes to give two independently movable single-beam gradient traps, the stiffness of each being equalised with a λ/2 plate. Either a 63×1.25 N.A. (Zeiss Antiflex Neofluor, 42 18 00) or a 63×1.40 N.A. (Zeiss Plan-Apochromat, 44 07 62) oil-immersion objective lens was employed mounted on a PZT focusing device (Physik Instrumente), which allowed precision sub-micrometre movement over a range of 0–0.35 mm. Trap stiffness was routinely measured by a method utilising Stokes' Law, which was found to be in satisfactory agreement with methods employing the measured Brownian motion of the trapped bead and the corner frequency of the power spectral density [19], and was of the order of 0.1 pN/nm.

Beads were visualised by brightfield illumination using a CCD camera, and recorded onto videotape, KET1-beads and kettin-beads distinguished by making KET1-beads fluorescent using a coating of RITC and observing the fluorescence image with a separate CCD. Records were sampled at 1 kHz using a PC equipped with data acquisition hardware and software (Labview, NI). Movement of trap 1 was effected by a pair of acousto-optic modulators (AOMs) (Isle Optics), trap 2 by two galvanometer-driven mirrors (Cambridge Technology). The position of the two trapped beads was monitored by splitting and focussing the brightfield image onto two separate 1 mm diameter quadrant photodiode (QD) detectors (Photonics), the bead in trap 1 being held in a position-clamp centred on the corresponding detector, QD1 [20]. Extension was calculated directly from the signal of the other detector, QD2, the centre of whose image was located ~3 μm from that of QD1 in the object plane of the trapped beads. Calibration of the QD2 signal was calculated from the time-averaged signal response following 20–30 oscillations of bead 2 against bead 1 in the absence of a tether. Force was calculated from the feedback signal applied to trap 1 necessary to keep the position of bead 1 clamped, multiplied by the AOM deflection calibration and the measured stiffness of the trap. Zeroing the force and extension signals was performed retrospectively by an automated routine written in Matlab which located the point of bead contact manifest in distinct spikes of the force and extension traces (Fig. 1B).

2.4. Stretching protocols

For each experiment a single molecule tether of kettin was formed between two optically trapped beads by tapping a kettin-bead against a KET1-bead using a triangle-wave profile of 1–2 Hz and 100–200 nm amplitude. The length of kettin tethered between the beads was assumed to be the region bound by the two epitopes, consisting of 19 complete Ig domains. Once a tether was formed the molecule was subjected to repeated stretch–release cycles using triangle and square-wave profiles spanning a range of frequencies from 0.1 to 5 Hz and a range of amplitudes from 50 to 500 nm. All experiments were performed at room temperature in PBS, pH 7.4.

2.5. Data analysis

Edge detection was automated using a Chung–Kennedy filter algorithm [21] written in Matlab setting a detection threshold [22] to give the probability for false-negative detection of <0.02 and that for false-positive detection of $<2\times10^{-5}$. The region of the force–extension relationship obtained for triangle-wave profile stretches between adjacent detected steps, or between the origin and the first detected step, was fitted by a single freely jointed chain (FJC) entropic spring [23] such that an external force F is related to the extension (end-to-end length) x by:

$$x = L_c\left(\coth\left(\frac{FL_k}{k_BT}\right)-\frac{k_BT}{FL_k}\right)$$

Absolute temperature is T, where k_B is the Boltzmann constant. L_k and L_c are the Kühn and contour lengths respectively, parameters which are related to the structural state of the molecule. Fits were also applied on the same data for a single worm-like chain (WLC) model [24], and also for an entropic-enthalpic model based on a WLC but with the addition of a bulk modulus factor [25]. All fits were performed using custom-written Matlab routines based on downhill Simplex minimisation [26]. Observed steps in x and F were converted to equivalent changes in L_c, ΔL_c, using the FJC or WLC model as appropriate whilst assuming negligible change to L_k (or persistence length in the case of WLC) as has been observed from other stretch studies on titin [16,17]. The same data were also subjected to double FJC fits, namely two independent FJC springs arranged in series such that:

$$x = \sum_{i=1}^{2} L_{ci}\left(\coth\left(\frac{FL_{ki}}{k_BT}\right)-\frac{k_BT}{FL_{ki}}\right)$$

Fits to a double WLC model [14] were similarly applied. Each detected step in a given stretch half-cycle for triangle-wave profile stretches was assigned a number, n_u, being the order in which the step was observed on the half-cycle time series, e.g. $n_u=1$ being the first observed step, $n_u=2$ being the second, etc. The mean rate of loading, r, was calculated from a linear fit of the force time series for each stretch half-cycle. The most likely force, F_u*, at which an Ig unfolding event occurs for n_f serially linked folded Ig domains was modeled by a modification of Kramers' theory [27] with the formulation due to Evans and Ritchie [28] such that:

$$F_u^* = \frac{k_BT}{x_u}\log_e\left(\frac{rx_u}{n_fk_u(0)k_BT}\right)$$

x_u is the width of the activation barrier for the unfolding transition (equivalent to the distance through which a force must be applied to a folded Ig domain in order to make it unfold at a given observed rate for that force), and $k_u(0)$ is the spontaneous rate of unfolding for a single domain at zero force. It is assumed that $n_f = N-n_u$, where N is the number of serially linked folded Ig domains in the initial undenatured state of the peptide. N is taken to be the number of complete Ig domains bounded by the KET1 and KET2 epitopes (19).

For the release half-cycle the force at time t from the start of release is given approximately by $F(t) = F(0)-rt$, and Kramers' theory predicts a most likely force of refolding F_r* for an unfolded Ig domain of:

$$F_f^* = -\frac{k_BT}{x_f}\log_e\left(\frac{rx_f}{n_uk_f(0)k_BT}\right)$$

x_f is the width of the activation barrier for the refolding transition and $k_f(0)$ is the spontaneous rate of refolding at zero force.

2.6. Monte Carlo simulation of unfolding and refolding

A simulation algorithm was written in Matlab, modeling the Ig transitions as a simple two-state process [15] polling at 1 ms time intervals to calculate the probability of unfolding and folding based upon pre-set kinetic parameters. The probabilities were then compared with pseudo-random numbers between 0 and 1 to determine whether the transition had occurred. Estimates for persistence and contour lengths were based on the previous analysis of Section 2.5.

3. Results

3.1. Fits to polymer models

Tethers formed were either short-lived (breaking in <5 stretch–release cycles) or long-lived (lasting for several minutes over the duration of the experiment. Short-lived tethers were likely to be due to non-specific interactions between the kettin- and KET1-beads and were excluded from subsequent

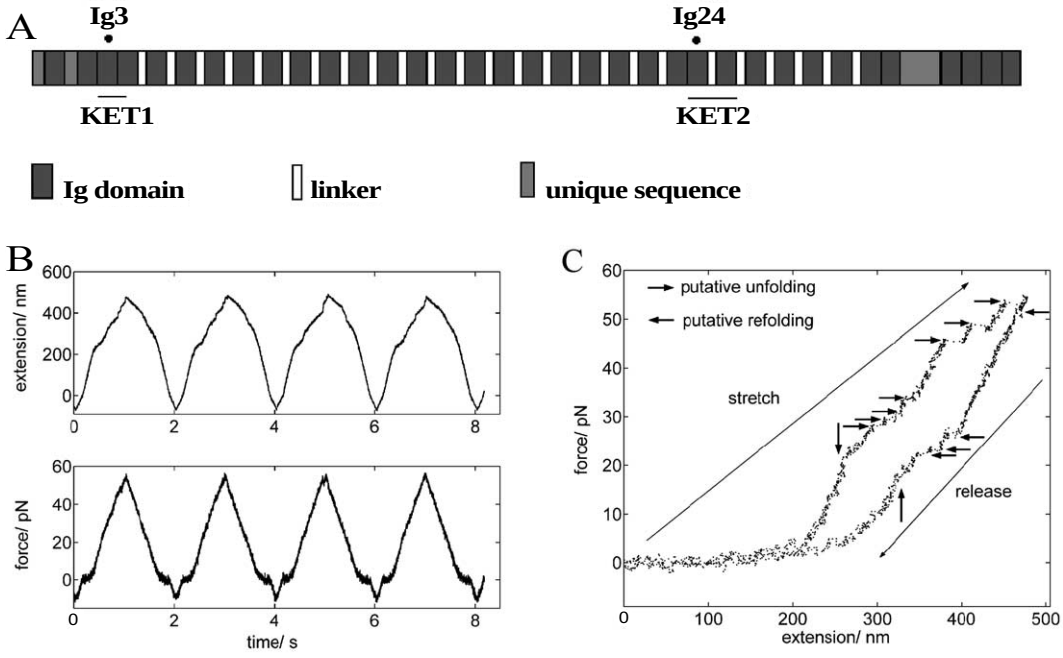

Fig. 1. A: Plan of the *Drosophila* kettin sequence. KET1 and KET2 are constructs to which antibodies have been raised. There are 19 complete Ig-linker modules between the two constructs. B: A typical time series for extension (upper) and force (lower) using low-pass filtered data, reflecting the outputs from QD2 and QD1 respectively. The location of some stress–relaxation events can be made out by eye, though identification was automated by a Chung–Kennedy edge detection routine. Within ~80% of forces around the midpoint between zero and maximum (~5 and ~50 pN in this instance) the variation of force is approximately linear with time, and the gradient of this straight-line fit was taken as the equivalent rate of loading. C: The majority of the first 10–20 single stretch–release cycles showed significant hysteresis, as with this example. Horizontal arrows mark the position of detected positive (stress–relaxation) and negative (recovery) steps, putatively due to unfolding and subsequent refolding of Ig domains. The high threshold of step detection set ensured that false-negatives were more likely than false-positives. The vertical arrows indicate distinct changes of slope that were not detected as steps and so most likely false-negatives.

analysis. Significant stress–relaxation and recovery were observed within the first 10–20 stretch–release cycles for the long-lived tethers (Fig. 1B,C). The latter figure also shows short regions in the force–extension relation on both stretch and release of changes in slope from expected non-linear to a more linear behaviour. This was consistent with Monte Carlo simulations in which two or more Ig domains had unfolded or refolded in relatively rapid succession of each other (less than the 20 ms running time window of the Chung–Kennedy filter), and which would pass undetected from the detection algorithm.

Applying a single FJC fit (Fig. 2A) to the force–extension relationship obtained between adjacent detected steps (or between the origin and the first detected step) Kühn lengths from 0.5 to 4.2 nm and contour lengths from 250 to 550 nm (circle symbol, Fig. 2B). Fits with a WLC were not significantly better than with a FJC generating persistence lengths smaller than the equivalent Kühn lengths by a factor of 1.5–2. Fitting with the entropic-enthalpic model did not produce significant improvements to the FJC or WLC, suggesting that the elasticity could be adequately modeled by a pure entropic spring. As the same figure shows, fitting these small segments of the force–extension relationship with a double serial FJC generates Kühn lengths of 0.2–1.4 nm for one chain and 5–13 nm for the other, with contour lengths of 50–600 nm and 50–350 nm respectively implying a total contour length of 300–650 nm.

3.2. Size and force dependence of step events

Conversion of the observed steps in x and F to an equivalent change in contour length generates two peaks in the distribution (Fig. 2C), one at ~+30 nm, similar to that observed from previous single molecule stretch studies of modular proteins containing Ig-like domains [14,16,17], and another at ~−30 nm, hitherto unresolved from other studies. Positive steps were detected over a force range of ~15–60 pN. Negative steps were detected at a force of 3–30 pN.

The maximum number of positive steps detected in any given stretch half-cycle for triangle-wave stretches was 15, whereas no more than five negative steps were detected in any release half-cycle. No positive steps were detected in any release half-cycle, and no negative steps in any stretch half-cycle, also the number of observed negative steps was always less than the number of positive steps detected from the previous stretch half-cycle.

The rate of loading, r, was in the range 5–100 pN/s. From the modified Kramers' theory above:

$$F_u^* = \frac{k_B T}{x_u}\log_e\left(\frac{r}{N-n_u}\right) + \frac{k_B T}{x_u}\log_e\left(\frac{x_u}{k_u(0)k_B T}\right)$$

Thus a linear fit (Fig. 2D) of the force at which positive steps are detected (putative unfolding) versus $\log_e\{r/(N-n_u)\}$ should yield both x_u and $k_u(0)$. The results from this (mean ± S.E.M.) are:

$$x_u = (0.29 \pm 0.01)\ \text{nm}$$

and

$$k_u(0) = (5.6 \pm 3.5)\times 10^{-3}\ \text{s}^{-1}$$

The value for x_u is in good agreement with atomic force

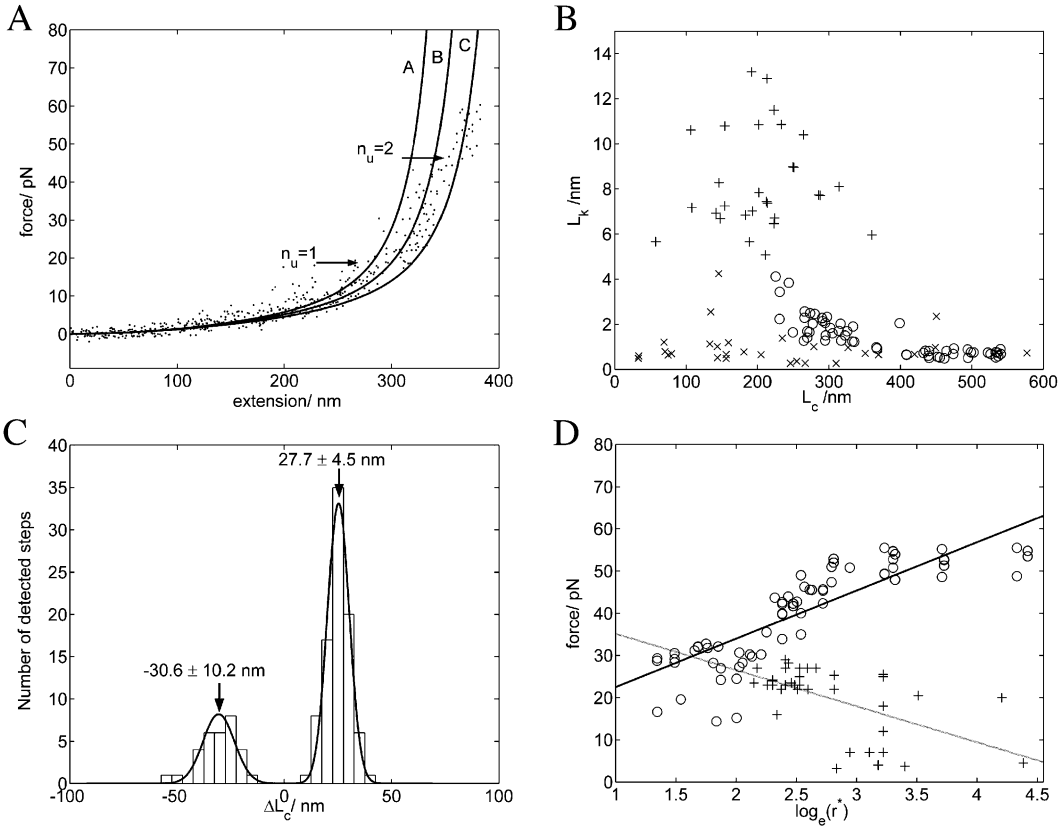

Fig. 2. A: The segment of unfiltered force–extension data illustrates the designation of n_u, arrows show positions of detected steps. Dotted curves are FJC fits to the inter-step regions of the force–extension relationship; curve A is a fit between the origin and the $n_u = 1$ step (no Ig domains unfolded prior to step), curve B to the one-domain-unfolded region between steps $n_u = 1$ and $n_u = 2$ and curve C to the two-domains-unfolded region data between the $n_u = 2$ step and the maximum extent of the stretch. B: The relation between Kühn and contour length for FJC fits applied to all inter-step regions of the force–extension traces, '○' for single FJC fits, 'x' for the small Kühn length component of the double FJC fit, '+' for the large Kühn length component of the double FJC fit. Simulations suggested typical errors of 5–10% on the contour length and 10–15% on Kühn length. Double FJC fits on very small segments of the force–extension relation resulted in artefactual convergence of one of the fitting parameters to an imposed boundary condition in the fitting algorithm and were treated as untrue solutions and not displayed here. A total of 117 step events were detected from 11 different bead pairs. C: Distribution of contour length step sizes using 5 nm bins. The curve shows the result of an unconstrained 2-Gaussian fit. Errors quoted represent the width of the corresponding Gaussian. D: Variation of measured force at which stress–relaxation ('○' with solid line fit) and recovery ('+' with dashed line fit) steps were detected versus log(r^*), where r^* is the rate of loading divided by either n_u (for recovery events) or $n_f = N - n_u$ (for stress–relaxation events).

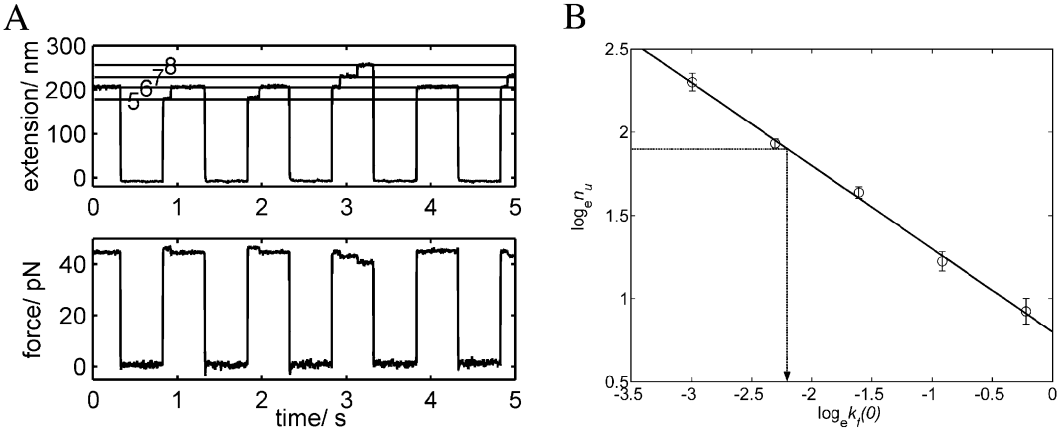

Fig. 3. A: Low-pass filtered data for a typical 1 Hz square wave stretch for extension (upper) and force (lower) versus time. The value of n_u was assigned at each different level of extension (the dotted lines show levels at 5, 6, 7 and 8) following the initial assignment of the $n_u = 1$ state defined as the first observed positive extension step in the stretch sequence. B: The graph shows a log–log plot of the predicted steady-state high force value of n_u versus $k_f(0)$ for a Monte Carlo simulation of the Ig unfolding and refolding processes for a continuous square wave stretch of 1 Hz and amplitude 40 ± 5 pN. Polling was performed at intervals of 1 ms. Extrapolation of the steady-state value from actual data (arrow) suggests a $k_f(0)$ of $\sim 0.11\ s^{-1}$.

microscopy stretch studies of tandem Ig or Fn3 domain constructs, for example, 0.3 ± 0.1 nm for the regions of titin covering Ig domains I27–I34 [16] and the Ig/Fn3 domains I48–I54 [17], 0.55 ± 0.1 nm for a 15 Fn3 domain region of the extracellular matrix protein tenascin [17], and 0.25 nm for titin domain I27 [29].

Similarly, a plot of the force at which negative steps are detected (putative refolding) versus $\log_e(r/n_u)$ for the refolding transition during the release half-cycle can be modeled by a linear fit of gradient $-k_B T/x_f$:

$$x_f = (0.48 \pm 0.06) \text{ nm (mean} \pm \text{S.E.M.)}$$

It is smaller than has been deduced from titin Ig modules by a factor of ~ 4 [29]. $k_f(0)$ was derived by a more direct method in preference to the interpolation approach with its large associated error. Tethers were stretched using a square-wave profile of 1 Hz, with amplitude of 40–50 pN (Fig. 3A). Relatively small fluctuations in n_u were observed between adjacent cycles suggesting a steady state had been reached, giving a mean of 6.7 ± 0.4 from three separate tethers. Monte Carlo simulations using the values above for x_u, $k_u(0)$ and x_f, and trying values of $k_f(0)$ between 0.05 and 0.80 s^{-1} produced a straight line on a log–log plot (Fig. 3B):

$$k_f(0) = (0.11 \pm 0.03)\ s^{-1} \text{ (mean} \pm \text{S.E.M.)}$$

4. Discussion

Polymer modeling shows evidence for two entropic chains acting in series in the KET1–KET2 antibody-delimited region of the kettin molecule. The size of the smaller Kühn length component is close to the contour length of two amino acid residues and suggests a possible basis in the flexibility of the linker regions. The larger Kühn length chain is much closer to the size of one to two Ig domains [30] and could therefore be due to the domains themselves. There is however a discrepancy between maximum measured contour length here (650 nm) and that predicted from sequence due to the unfolding of a maximum of 15 Ig domains (797 nm). This is likely to be related to some unanticipated interaction between bead, antibody and kettin. Immunoelectron microscopy experiments on insect myofibrils confirmed a high degree of specificity for the antibodies used, and estimations of antigen–antibody dissociation constants from surface plasmon resonance with a width of activation potential of 0.4 nm [31] suggested typical unbinding forces in excess of 90 pN at the rates of loading used here, so it seems unlikely that the discrepancy is due to a problem of non-specificity, or of the antibody detaching from its epitope under stress. Suggestions of incomplete unfolding are also unlikely since the measured peak in the size of the putative unfolding event (~ 30 nm) is consistent with that expected from sequence, unless there is some undetected incomplete refolding of the domain following the unfolding event. What is more likely is that a length of kettin between the epitope sites remains weakly bound to the bead at low force and then breaks off at higher forces, manifest in a false Ig stress–relaxation event, such that the maximum value of 15 putative unfolding steps is an overestimate, with 10 or 11 being more consistent with the calculated contour length from sequence data.

The comparatively large spontaneous rate of unfolding indicates a lower stability in the folded Ig structure compared to many of the Ig domains of titin. The rate of refolding at zero force is comparable to titin Ig domains, however the width of the refolding activation barrier is smaller than that estimated for the I27 domain of titin by a factor of ~ 4 [29], the implication being that refolding can occur at higher forces for equivalent rates of loading. This may favour a role as shock-absorber, similar to that suggested for titin Ig domains in the vertebrate sarcomere. A potentially damaging stretch on the insect sarcomere could cause one or more Ig domains to unfold thereby allowing the sarcomere to extend and accommodate the extra tension, reducing potential damage to the thick and thin filaments. The ability for these unfolded domains to then refold at relatively high forces is a possible selective advantage since normal functioning of the sarcomere can resume without requiring it to be effectively slack. It is also possible that the mechanical function of kettin reaches beyond a mere shock-absorber; since domain refolding occurs at unprecedentedly high forces we can speculate that kettin may well function as a highly efficient folding-based spring with relatively little force hysteresis.

Acknowledgements: The authors would like to thank the BBSRC, MRC, HFSP and EU for their generous support of this work.

References

[1] Lakey, A., Ferguson, C., Labeit, S., Reedy, M., Larkins, A., Butcher, G., Leonard, K. and Bullard, B. (1990) EMBO J. 9, 3459–3467.
[2] Lakey, A., Labeit, S., Gautel, M., Ferguson, C., Barlow, D.P., Leonard, K. and Bullard, B. (1993) EMBO J. 12, 2863–2871.
[3] Hakeda, S., Endo, S. and Saigo, K. (2000) J. Cell Biol. 148, 101–114.
[4] Kolmerer, B., Clayton, J., Benes, V., Allen, T., Ferguson, C., Leonard, K., Weber, U., Knekt, M., Ansorge, W. and Labeit, S. et al. (2000) J. Mol. Biol. 296, 435–448.
[5] van Straaten, M., Goulding, D., Kolmerer, B., Labeit, S., Clayton, J., Leonard, K. and Bullard, B. (1999) J. Mol. Biol. 285, 1549–1562.
[6] Bullard, B. and Leonard, K. (1996) Adv. Biophys. 33, 211–221.
[7] Kulke, M., Neagoe, C., Kolmerer, B., Minajeva, A., Hinssen, H., Bullard, B. and Linke, W.A. (2001) J. Cell Biol. 154, 1045–1057.
[8] Machado, C. (2000) J. Cell Biol. 151, 639–652.
[9] Zhang, Y., Featherstone, D., Davis, W., Rushton, E. and Broadie, K. (2000) J. Cell Sci. 113, 3103–3115.
[10] Labeit, S. and Kolmerer, B. (1995) Science 270, 293–296.
[11] Freiberg, A., Trombitas, K., Hell, W., Cazorla, O., Fougerousse, F., Centner, T., Kolmerer, B., Witt, C., Beckmann, J.S., Gergorio, C.C., Granzier, H. and Labeit, S. (2000) Circ. Res. 86, 1114–1121.
[12] Daley, J., Southgate, R. and Ayme-Southgate, A. (1998) J. Mol. Biol. 279, 201–210.
[13] Southgate, R. and Ayme-Southgate, A. (2001) J. Mol. Biol. 313, 1035–1043.
[14] Tskhovrebova, L., Trinick, J., Sleep, J.A. and Simmons, R.M. (1997) Nature 387, 308–312.
[15] Kellermayer, M.S., Smith, S.B., Granzier, H.L. and Bustamante, C. (1997) Science 276, 1112–1116.
[16] Rief, M., Gautel, M., Oesterhelt, F., Fernandez, J.M. and Gaub, H.E. (1997) Science 276, 1109–1112.
[17] Rief, M., Gautel, M., Schemmel, A. and Gaub, H.E. (1998) Biophys. J. 75, 3008–3014.
[18] Minajeva, A., Kulke, M., Fernandez, J. and Linke, W. (2001) Biophys. J. 80, 1442–1451.
[19] Svoboda, K. and Block, S.M. (1994) Annu. Rev. Biophys. Biomol. Struct. 23, 247–285.
[20] Simmons, R.M., Finer, J.T., Chu, S. and Spudich, J.A. (1996) Biophys. J. 70, 1813–1822.
[21] Chung, S.H. and Kennedy, R.A. (1991) J. Neurosci. Methods 40, 71–86.

[22] Smith, D.A. (1998) Phil. Trans. R. Soc. Lond. B 353, 1969–1981.
[23] Smith, S.B., Cui, Y. and Bustamante, C. (1996) Science 271, 795–799.
[24] Marko, J.F. and Siggia, E. (1995) Macromolecules 28, 209–212.
[25] Odjik, T. (1995) Macromolecules 28, 7016–7018.
[26] Nelder, J.A. and Mead, R. (1965) Comput. J. 7, 308–313.
[27] Bell, G.I. (1978) Science 200, 618–627.
[28] Evans, E. and Ritchie, K. (1997) Biophys. J. 72, 1541–1555.
[29] Carrion-Vazquez, M., Oberhauser, A.F., Fowler, S.B., Marszalek, P.E., Broedel, S.E. and Clarke, J. (1999) Proc. Natl. Acad. Sci. USA 96, 3694–3699.
[30] Pfuhl, M., Gautel, M., Politou, A.S., Joseph, C. and Pastore, A. (1995) J. Biomol. NMR 6, 48–58.
[31] Schwesinger, F., Ros, R., Struntz, T., Anselmetti, D., Guntherodt, H.J., Honegger, A., Jermutus, L., Tiefenauer, L. and Pluckthun, A. (2001) Proc. Natl. Acad. Sci. USA 97, 9972–9977.
[32] Bullard, B., Linke, W.A. and Leonard, K. (2002) J. Muscle Res. Cell Motil. (in press).